Inorganic Chemistry

ARTICLE

pubs.acs.org/IC

$LiSbO_2$: Synthesis, Structure, Stability, and Lithium-Ion Conductivity

Benjamin P. de Laune, Ryan D. Bayliss,† and Colin Greaves*

School of Chemistry, University of Birmingham, Birmingham B15 2TT, U.K.

Supporting Information

ABSTRACT: $LiSbO_2$ has been synthesized using a ceramic method involving evacuated quartz tubes to ensure stoichiometry. Its structure [monoclinic, $P2_1/c$; a = 4.8550(3) Å, b = 17.857(1) Å, c = 5.5771(3) Å; β = 90.061(6)°] has been determined using X-ray and neutron diffraction and refined on the basis of neutron data. The structure is significantly different from that of $LiBiO_2$ and contains chains of corner-linked SbO_3 trigonal pyramids, which provide a framework for the tetrahedral coordination of Li^+ ions. A layer structure results in which the Li sites are located in planes perpendicular to [010]. $LiSbO_2$ is stable in air up to ca. 400 °C, but at higher temperatures, oxidation to $LiSbO_3$ occurs as a two-stage process, with evidence for a metastable, intermediate $LiSbO_{2.5}$ phase presented. The Li^+-ion conductivity, measured using alternating-current impedance spectroscopy, is similar to that of $LiBiO_2$, with a value of ca. 10^{-6} S cm^{-1} at 300 °C.

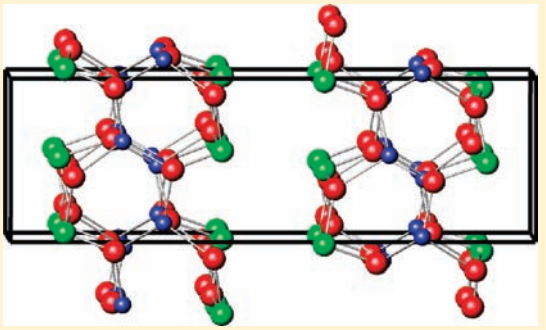

INTRODUCTION

An important feature of the structural chemistry of arsenic(III), antimony(III), and bismuth(III) oxides is the influence of the lone pair of electrons on the cation. This provides asymmetric environments for the cations, and the space occupied by the lone pair provides an expanded structure that can give rise to important properties such as exceptionally high ionic conductivity, as exhibited by the disordered, high-temperature form of Bi_2O_3, δ-Bi_2O_3.[1] Many oxides ABO_2 (A = alkali metal; B = As, Sb, Bi) exist with low-dimensional structural features that reflect the bonding preferences of the cation B.[2−13] These oxides are summarized in Table 1 and have three basic structures:

M = *monoclinic*, $C2/c$ (e.g., $NaBiO_2$)

O-I = *orthorhombic*, *Ibam* ($LiBiO_2$)

O-II = *orthorhombic*, *Pbca* (e.g., $NaAsO_2$)

The structures of all three reported $AAsO_2$ materials are very similar, in spite of the space group for A = Na (*Pbca*) being different from that of A = K, Rb (*Pbcm*).[2]

Table 1 indicates that the heavier A and B cations prefer the M structure, which does not contain discrete BO_2 layers, in contrast to the O-I and O-II structures (vide infra). The M structure contains B cations bonded to four O atoms in a pseudo-trigonal-bipyramidal arrangement if the lone-pair electrons are included in the coordination polyhedron. The BO_4 polyhedra are linked through edges to form chains, with the interstices between the chains providing the locations for the A cations. Figure 1a shows the arrangement for $NaBiO_2$.[7,10] The O-I structure is adopted by $LiBiO_2$ and contains discrete BiO bilayers that are separated by Li ions in tetrahedral coordination. In the ideal structure, each Bi^{3+} cation has square-pyramidal coordination, with the pyramid base lying in the BiO plane with the fifth, apical, O atom pointing into the region containing the Li ions. This arrangement is shown in Figure 1b. However, this ideal model based on X-ray diffraction appears incomplete and resulted in a poor refinement with unacceptable displacement parameters in a subsequent neutron powder diffraction (NPD) study.[14] On the basis of a more detailed NPD investigation, it was suggested that the structure is, in fact, locally distorted to give three short Bi−O bonds and trigonal-pyramidal coordination for Bi; the local structure is probably consistent with *Iba*2 symmetry.[3] The $AAsO_2$ compounds contain AsO layers, but in contrast to the larger antimony and bismuth oxides, each layer comprises chains of corner-linked AsO_3 trigonal pyramids.[2,8,9] For each AsO_3 unit, two O atoms in the layer are bridging with the third O atom directed outward to allow bonding to the alkali A cations. The links within the chains provide a zigzag arrangement, as shown in Figure 1c, and the chains provide for seven-coordinate (A = Na) or eight-coordinate (A = K, Rb) A cations.

It is surprising that detailed structures have not been reported for ternary oxides of lithium with the smaller As^{3+} or Sb^{3+} cations. Although it has been implied that $LiSbO_2$ and $LiBiO_2$ are isostructural,[15,16] we are aware of no published evidence for this. Moreover, this is in conflict with an earlier single-crystal study using a crystal obtained from a LiCl/KCl flux.[17] This study suggested an orthorhombic unit cell (a = 4.068 Å, b = 9.790 Å, and c = 5.650 Å) with space group *Pmmn* or $P2_1mn$, in marked contrast to the structure of $LiBiO_2$: *Ibam*, a = 17.976(4) Å,

Received: June 1, 2011
Published: July 19, 2011

Table 1. Structural Summary for Phases ABO_2

	As	Sb	Bi
Li			O-I[3,6]
Na	O-II[2,8,9]		M[7,10]
K	O-II[a,2]	M[4]	M[7,11,12]
Rb	O-II[a2]	M[4]	M[7,12]
Cs		M[5]	M[7,13]

[a] These materials have a slightly different structure from O-II with *Pbcm* symmetry.

$b = 5.179(1)$ Å, and $c = 4.972(1)$ Å.[3] In fact, the suggested unit cell seems incompatible with all three structures described briefly above (M, O-I, and O-II), but, unfortunately, Sauvage et al.[17] provided no further structural characterization for their crystal. In order to resolve this anomaly, a pure sample of $LiSbO_2$ has been synthesized in powder form and its structure determined using NPD data. Its stability to air oxidation and its ionic conductivity properties have also been investigated and are reported.

EXPERIMENTAL SECTION

Samples of $LiSbO_2$ were synthesized from an intimate mixture of Sb_2O_3(Sigma-Aldrich, 99%) and Li_2O (Sigma-Aldrich, 97%, in 5% excess) contained in silver tubes with crimped ends. The tubes were placed in quartz tubes, evacuated, and heated at 500 °C for periods of 48 and 72 h with an intermediate regrind. All grinding and weighing was carried out in a glovebox under an atmosphere of pure-shield argon. Sb_2O_3 was dried under a dynamic vacuum at 150 °C for at least 4 h prior to use.

Powder X-ray diffraction (PXRD) patterns were obtained using a Bruker D8 diffractometer (Cu $K\alpha_1$, $\lambda = 1.5406$ Å, from a primary beam Ge monochromator and a Lynxeye detector in transmission geometry), and variable-temperature PXRD (VT-PXRD) data were collected in air on a Siemens D5005 (Cu $K\alpha$, $\lambda = 1.5418$ Å, Braun PSD, with an Anton-Parr heating stage) in reflection geometry. Powder patterns were indexed using the program *DICVOL06*.[18] NPD data were obtained at ambient temperature on the HRPT diffractometer at SINQ, PSI, Zurich, Switzerland ($\lambda = 1.4942$ Å), using 8 mm diameter vanadium cans. Neutron scattering lengths assigned to Li, Sb, and O were −1.90, 5.57, and 5.81 (all $\times 10^{-15}$ m). The general structure analysis program *GSAS*[19] was used for structure refinements in conjunction with the user interface *EXPGUI*.[20] A pseudo-Voigt peak-shape function was used, and the background was fitted using linear interpolation.

Thermogravimetric analysis (TGA) and differential thermal analysis (DTA) were performed on a Netzsch Sta 449 F1 analyzer in an atmosphere of O_2 and at a heating rate of 10 °C min^{-1}. Alternating-current (ac) impedance measurements were performed using a Solartron SI 1260 impedance analyzer under variable-temperature conditions in air. A cylindrical pellet of 8 mm diameter was used (obtained by uniaxial pressing at 0.5 tonne to give a density of 82% of theoretical) with its faces coated with silver paste; contacts to the faces utilized spring-tensioned electrodes. The crystal morphology was determined via scanning electron microscopy (SEM) using a JEOL 6060 instrument.

RESULTS AND DISCUSSION

Structural Determination and Refinement. Sauvage et al.[17] presented no structure solution for their sample, assumed to be $LiSbO_2$, but relative peak intensity data were provided that allowed a simulation of the powder pattern; this clearly indicated a totally different structure from that of the material synthesized in the current study using ceramic methods. It is possible that the

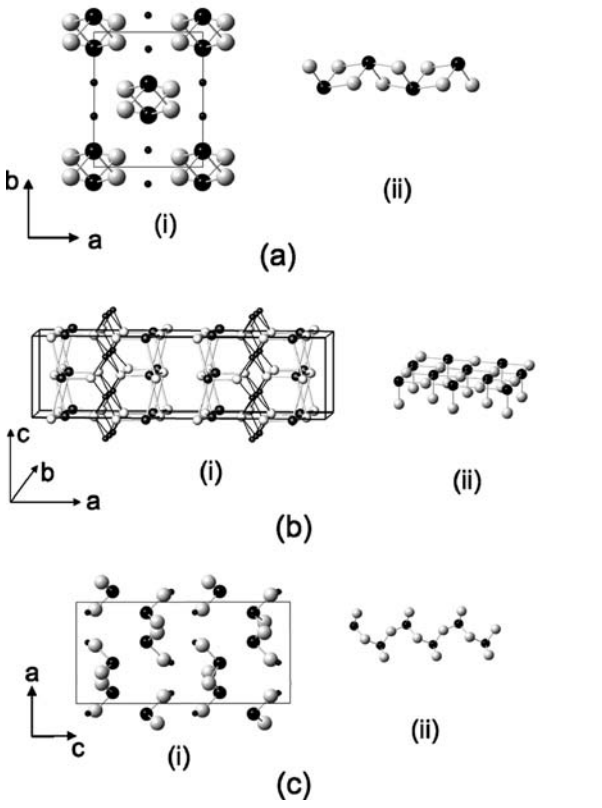

Figure 1. Structures of (a) $NaBiO_2$,[7,10] (b) $LiBiO_2$,[3,6] and (c) $NaAsO_2$.[2,8,9] (a) M structure of $NaBiO_2$: (i) a projection along [001] showing the channels that accommodate the A cations; (ii) a BiO_2 chain viewed approximately perpendicularly to [010] and [001] and containing edge-linked BiO_4 trigonal bipyramids (O, white spheres; Bi, large black spheres; A, small black spheres]. (b) O-I structure of $LiBiO_2$: (i) a projection approximately along [010] showing the layers of tetrahedrally coordinated Li ions (small black spheres); (ii) the BiO_2 layers containing edge-linked BiO_5 square pyramids (O, white spheres; Bi, large black spheres).(c) O-II structure of $NaAsO_2$: (i) a projection along [010] showing the layers that contain the chains of linked AsO_3 trigonal pyramids (Sb, large black spheres; O, white spheres) directed along [010]. The A cations (small black spheres) are seven-coordinate (A = Na) or eight-coordinate (A = K, Rb). (ii) AsO_2 chain containing corner-linked AsO_3 trigonal pyramids (O, white spheres; Bi, large black spheres) viewed along [001].

structure of the flux-grown crystal corresponds to a lower-temperature polymorph or a partially oxidized composition (vide infra). In the current study, indexing of the PXRD data was possible using an orthorhombic cell that appeared to be related to that of $LiBiO_2$, with $a = 17.83$ Å, $b = 5.57$ Å, and $c = 4.85$ Å. However, the indexing was incompatible with the *Ibam* space group of $LiBiO_2$, and a primitive cell was indicated; absences suggested possible $P2_12_12_1$ symmetry, which allowed generation of the basic features of the $LiBiO_2$ structure and retained 2_1 elements along all axes. For Rietveld refinement, only Sb and O atoms were included because of the small X-ray scattering factor for Li. Satisfactory refinement required a correction (March-Dollase) for the preferred orientation along [100], consistent with crystal platelets with faces perpendicular to [100]. The final fit [Figure S1 in the Supporting Information; $\chi^2 = 3.021$, $a = 17.8316(6)$ Å, $b = 5.5678(1)$ Å, and $c = 4.8477(1)$ Å] suggested that the space group allowed reasonable modeling of the Sb−O

dx.doi.org/10.1021/ic201183e |*Inorg. Chem.* 2011, 50, 7880–7885

framework and that large structural differences, therefore, existed between the current sample and that examined by Sauvage et al.[17]

NPD data at 300 K, however, could not be fitted satisfactorily using this model (Figure S2 in the Supporting Information). Given the small neutron scattering length for Li and the satisfactory PXRD fit, it was clear that the deficiency in the model related primarily to the O atom positions being incompatible with the $P2_12_12_1$ space group. It was concluded that the structures of $LiSbO_2$ and $LiBiO_2$ were significantly different, and a lower symmetry, monoclinic space group was, therefore, sought. $P2_1/c$ was favored (with 2_1 along the long axis) because it is the highest-symmetry monoclinic maximal subgroup of *Pbam* ($LiBiO_2$ symmetry after removal of the I-centring). The ideal orthorhombic cell above then transforms to $P2_1/c$ with a = 4.8477(1) Å, b = 17.8316(6) Å, c = 5.5678(1) Å, and β = 90°. Initially, the Li atoms were excluded because of their limited contribution to the profile, and the refinement proceeded in a straightforward fashion to yield a reasonably good fit (χ^2 = 7.219), which supported the space group assignment. The location of the Li atoms was then investigated using difference Fourier methods. Despite the small neutron scattering length for Li, a negative scattering intensity was found in two, symmetry-unrelated, positions that seemed sensible for such ions (Figure S3 in the Supporting Information). Moreover, incorporation of Li at the suggested positions resulted in a significant improvement to the refinement. The final fit (Figure 2; χ^2 = 1.849 and R_{wp} = 0.0476) corresponds to all atomic positions and isotropic displacement parameters being refined independently (Table 2); a small correction for the preferred orientation was necessary. The monoclinic distortion, as reflected in unit cell dimensions, is small [β = 90.061(6)°]. Given the relatively small lithium content, no correction was applied for absorption, and the displacement parameters, which would be correlated with absorption effects, are all reasonable.

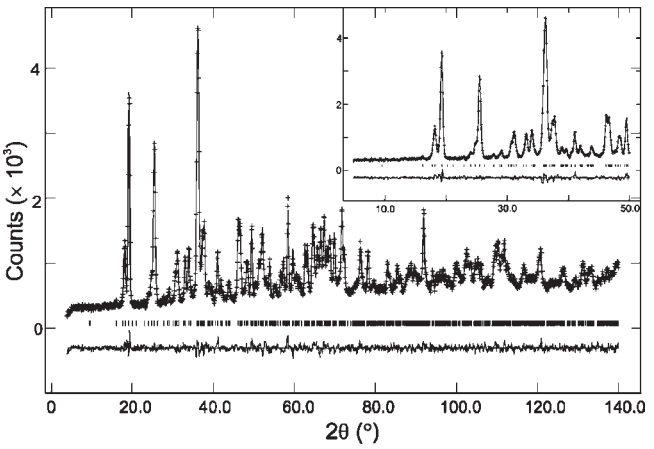

Figure 2. Final Rietveld refinement based on ambient-temperature NPD data using $P2_1/c$ showing observed data (+), calculated and difference profiles (continuous lines), and reflection positions (|). The inset shows a more detailed plot for 10° < 2θ < 50°.

Table 2. Refinement Structural Parameters for $LiSbO_2$ (All Atoms in 4e Sites)[a]

atom	x	y	z	$100U_{iso}$/Å^2
Sb1	0.259(2)	0.5994(4)	0.5711(8)	1.1(2)
Sb2	0.237(2)	0.4032(4)	0.994(1)	0.7(1)
O1	0.339(1)	0.6942(4)	0.463(1)	0.9(1)
O2	0.170(2)	0.3034(6)	0.878(1)	2.0(2)
O3	0.367(1)	0.6167(5)	0.920(1)	1.2(2)
O4	0.138(1)	0.3848(5)	0.333(1)	1.4(2)
Li1	0.254(5)	0.219(1)	0.042(3)	1.6(5)
Li2	0.770(5)	0.211(1)	0.376(3)	0.9(4)

[a] a = 4.8550(3) Å; b = 17.857(1) Å; c = 5.5771(4) Å; β = 90.061(6)°.

Structure Description. The crystal structure (Figure 3a) comprises isolated chains of corner-sharing SbO_3 trigonal-pyramidal units, propagating along [100] (Figure 3b), and provides an overall layer structure with [010] perpendicular to the layers. Two distinct types of Sb−O bonds exist: each Sb is bonded to one terminal (nonbridging) O atom (O1 to Sb1 and O2 to Sb2) and two bridging atoms, O3 and O4. The terminal O atoms project from the Sb−O backbone and are aligned approximately in the [010] direction, as shown in Figure 3a. Regions containing opposing Sb1−O1 and Sb2−O1 bonds, at planes with y = 0.25 and 0.75, accommodate the Li ions in tetrahedral coordination (Figure 3c). The structure is closely related to that of $NaAsO_2$,[2,8,9] in which the Na ions have four short tetrahedrally coordinated bonds and three longer bonds; however, $NaAsO_2$

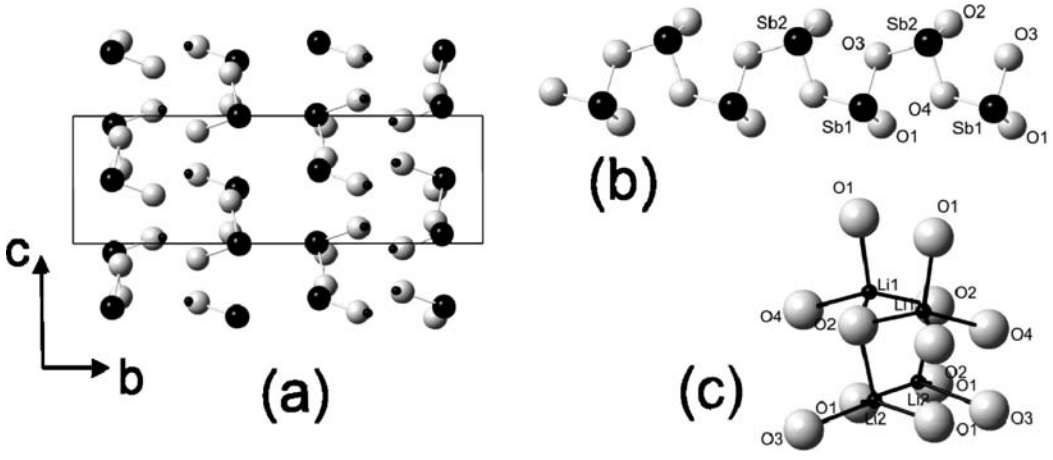

Figure 3. Structure of $LiSbO_2$ (Li, small black spheres; Sb, large black spheres; O, white spheres): (a) structure projected along [100] showing the SbO_2 chains end-on; (b) linking of the SbO_3 trigonal-pyramidal units to form SbO_2 chains parallel to [100]; (c) tetrahedral coordination of the two Li sites.

dx.doi.org/10.1021/ic201183e |*Inorg. Chem.* 2011, 50, 7880–7885

Table 3. Selected Bond Lengths and Angles

bond lengths/Å		angles/deg	
Li1−O1	2.03(3)	O1−Li1−O2	113(1)
Li1−O2	1.81(2)	O1−Li1−O2	100(1)
Li1−O2	1.96(2)	O2−Li1−O2	128(1)
Li1−O4	2.26(2)	O1−Li1−O4	93.1(9)
		O2−Li1−O4	111.5(9)
		O2−Li1−O4	106(1)
Li2−O1	1.98(2)	O1−Li2−O1	119(1)
Li2−O1	1.99(2)	O1−Li2−O2	104.5(8)
Li2−O2	1.96(2)	O1−Li2−O2	112(1)
Li2−O3	2.14(2)	O1−Li2−O3	108(1)
		O1−Li2−O3	110(2)
		O2−Li2−O3	101.7(9)
Sb1−O1	1.84(1)	O1−Sb1−O3	96.9(4)
Sb1−O3	2.036(8)	O1−Sb1−O4	99.2(5)
Sb1−O4	2.02(1)	O3−Sb1−O4	88.3(3)
Sb2−O2	1.92(1)	O2−Sb2−O3	94.5(4)
Sb2−O3	2.02(1)	O2−Sb2−O4	97.3(4)
Sb2−O4	1.978(9)	O3−Sb2−O4	88.6(4)

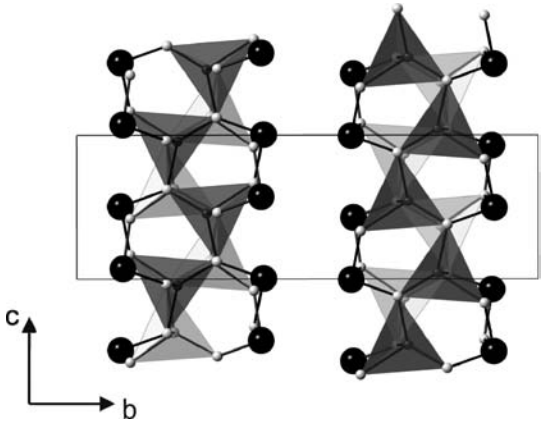

Figure 4. $LiSbO_2$ viewed along [100] showing alternation of Li1 (light gray) and Li2 (dark gray).

has orthorhombic symmetry (*Pbca*). Bond distances and angles are shown in Table 3. The LiO_4 tetrahedra are seen to be distorted, with a larger distortion occurring for Li1 than Li2. For any Li-rich plane, e.g., $y = 0.25$, the Li ions are ordered to provide alternating sheets of Li1 and Li2 tetrahedra perpendicular to [100], as seen in Figure 4. The Sb^{3+} lone pairs of electrons are presumably directed into the layer regions within the unit cell at $y = 0$ and 0.5.

As seen in Table 3, the terminal Sb−O bonds [1.84(1) and 1.92(1) Å] are significantly shorter than the bridging bonds [1.978(8)−2.036(8) Å], as expected. This is similar to that observed in $NaAsO_2$, with average terminal and bridging distances of 1.684(4) and 1.822(3) Å, respectively.[8] The O−Sb−O bond angles are all very much less than that for tetrahedral coordination (including the lone pair) and reflect the repulsive influence of the lone pair of electrons. In addition, the O−Sb−O angles within the chains are approximately 6−10° larger than the angles involving a terminal O1 or O2 atom, consistent with a greater electronic repulsion provided by the electrons in the shorter terminal bonds.

Table 4. BVS Values Based on the Data Obtained from NPD Data

atom	BVS	atom	BVS
Li1	0.99	Sb1	3.19
Li2	0.93	Sb2	3.00

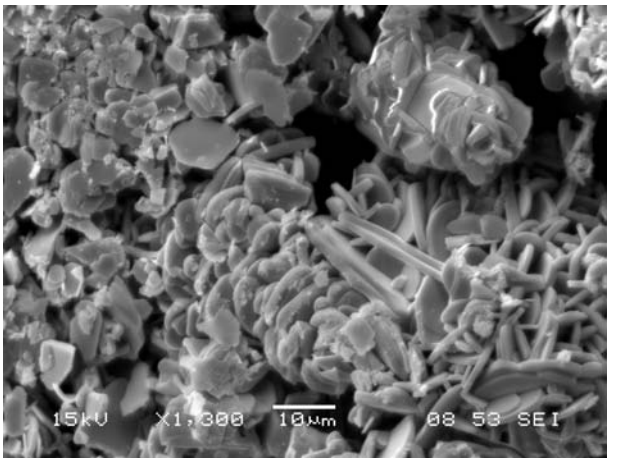

Figure 5. SEM micrograph showing platelets with faces typically ~10 μm in diameter.

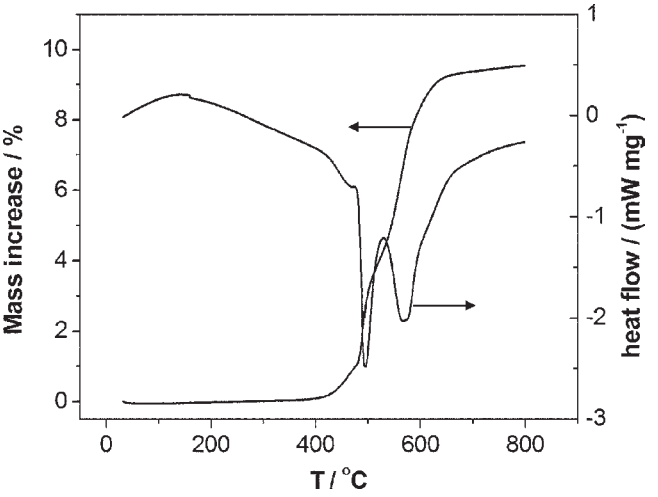

Figure 6. TGA and DTA traces corresponding to the heating of $LiSbO_2$ in oxygen.

Bond valence sum (BVS) calculations[21] were performed (Table 4) and support the validity of the structure with respect to cation-bonding requirements: calculated valences of Li and Sb are in good agreement with their idealized ionic charges.

The preferred orientation implied by PXRD and NPD structure refinements suggested a crystal morphology involving platelets with faces perpendicular to the monoclinic [010] direction. SEM analysis (Figure 5) confirmed this by showing crystal platelets with faces typically approximately 10 μm in diameter.

Thermal Stability. The thermal stability in oxygen was investigated because of the expected susceptibility of Sb^{3+} to

dx.doi.org/10.1021/ic201183e |*Inorg. Chem.* 2011, 50, 7880–7885

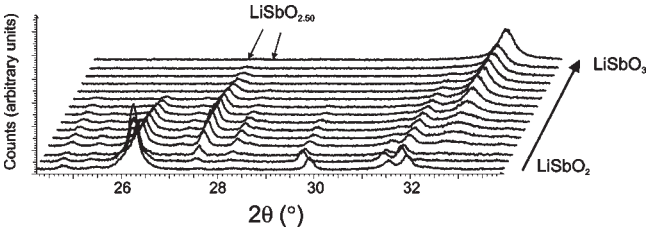

Figure 7. VT-PXRD traces for $LiSbO_2$ heated in air. The data have been electronically stripped of the $K\alpha_2$ component. The bottom and top traces correspond to the starting material ($LiSbO_2$) and product ($LiSbO_3$), respectively, at 25 °C. The intermediate plots are, from the botttom, at increasing temperatures between 400 and 580 °C in regular intervals of 15 °C.

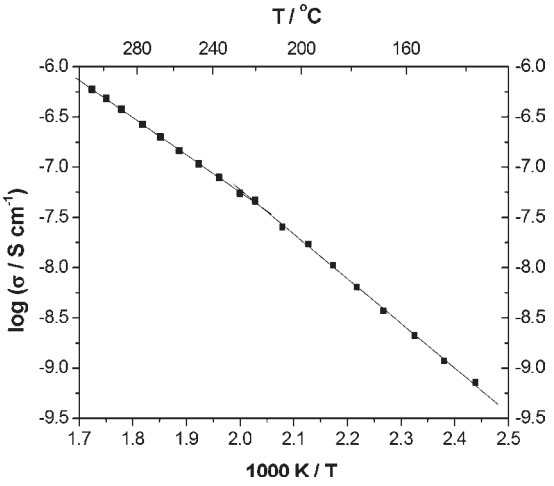

Figure 8. Variation of the conductivity of $LiSbO_2$ with temperature as measured by log σ vs $1000/T$. Linear fits to the data are shown for $T \leq 220$ °C and $T \geq 220$ °C.

aerial oxidation. The TGA data (Figure 6) show a mass increase of 9.6% to give the final product of $LiSbO_3$ at 800 °C, which was confirmed by PXRD; the expected mass increase is 10.0%. However, an intermediate plateau region at ca. 550 °C appears to correspond to a mixed Sb^{3+}/Sb^{5+} phase with empirical formula $LiSbO_{2.5}$. The occurrence of a two-stage oxidation process is confirmed by DTA data (Figure 6), which show two distinct and large exotherms with peaks at ca. 500 and 580 °C. Structural information on the intermediate phase was sought using VT-PXRD studies (Figure 7). A gradual transition from $LiSbO_2$ to $LiSbO_3$ in the range 400−580 °C can be seen, with the disappearance of intensity from the $LiSbO_2$ phase and the emergence of new peaks corresponding to poorly crystalline $LiSbO_3$. However, the presence of a few intermediate peaks (in particular, at 2θ values of 27.5° and 28.3°) that are absent in both $LiSbO_2$ and $LiSbO_3$ supports a two-stage transformation process. At present, attempts to synthesize the intermediate phase using sealed tube methods, assuming a composition of $LiSbO_{2.5}$, have proved impossible and suggest that the phase is probably metastable, and thermodynamically unstable at the synthesis temperatures required. It seems possible that the flux-grown crystal described by Sauvage et al.[17] could correspond to this partially oxidized phase.

Conductivity Measurements. Given the presence of layers of Li ions in the structure of $LiSbO_2$, its conductivity was measured using ac impedance measurements within its thermal stability range. PXRD was used to confirm that no oxidation had occurred during the measurements. The results are shown in Figure 8 and relate to the total (bulk and grain boundary) conductivity as determined from the low-frequency intercept with the real axis of the observed semicircles of the complex plane impedance plots. The Arrhenius plot shows two regions of straight-line behavior with slightly different activation energies: 0.88 eV below 220 °C and 0.74 eV above 220 °C. VT-PXRD data were unable to provide any indication as to the structural origin for this observation, and very careful variable-temperature NPD data would be required to provide meaningful information relating to changes in the Li environments. The conductivity behavior is similar to that previously reported for $LiBiO_2$,[14] with the conductivity of both being ca. 10^{-6} S cm^{-1} at 300 °C. The activation energy for $LiBiO_2$ was reported as 0.72 eV.[14] The conductivity, which is assumed to relate to Li^+-ion migration, is therefore very low and has an associated high activation energy. This is consistent with a highly ordered structure (no Li-ion vacancies) and a substantial jump distance of ∼3 Å between nearest-neighbor Li sites. Attempts were made to synthesize defective variants containing dopant cations of a suitable charge and affinity for tetrahedral geometry (Zn^{2+}, Al^{3+}, and Ga^{3+}) but were unsuccessful.

CONCLUSIONS

It has been demonstrated that $LiSbO_2$ has a monoclinic crystal structure [$P2_1/c$, $a = 4.8550(3)$ Å; $b = 17.857(1)$ Å; $c = 5.5771(4)$ Å; $\beta = 90.061(6)°$], which is stable in ambient conditions with minimal uptake of oxygen up to ca. 400 °C. The system is not isostructural to that of $LiBiO_2$ nor is it related to the compound previously reported as $LiSbO_2$ by Sauvage et al.[17] The compound is found to undergo a two-stage oxidation to $LiSbO_3$, with evidence for an intermediate mixed oxidation (Sb^{3+}/Sb^{5+}) phase of composition $LiSbO_{2.5}$. This phase appears metastable, and no structural details are available. The Li^+-ion conduction of $LiSbO_2$ is low and similar to that reported for $LiBiO_2$,[14] which has some similar structural features.

ASSOCIATED CONTENT

Supporting Information. Rietveld refinement and plane of the difference Fourier plot for NPD data. This material is available free of charge via the Internet at http://pubs.acs.org.

AUTHOR INFORMATION

Corresponding Author

*E-mail: c.greaves@bham.ac.uk. Tel: +44-121-4144397.

Present Addresses

[†]Department of Materials, Royal School of Mines, South Kensington Campus, Imperial College London, London SW7 2AZ, U.K.

ACKNOWLEDGMENT

We thank the EPSRC and University of Birmingham for financial support and Vladimir Pomjakushin for help with the collection of NPD data. The Bruker D8 diffractometer and the Netzsch STA 449 F1 Jupiter TGA instrument used in this research were obtained through Birmingham Science City: Creating and Characterising Next Generation Advanced

Materials (West Midlands Centre for Advanced Materials Project 1), with support from Advantage West Midlands and partial funding by the European Regional Development Fund.

REFERENCES

(1) Takahashi, T.; Iwahara, H. *Mater. Res. Bull.* **1978**, *13*, 1447–1453.
(2) Emmerling, F.; Röhr, C. *Z. Naturforsch.* **2003**, *58b*, 620–626.
(3) Greaves, C.; Katib, S. M. A. *J. Chem. Soc., Chem. Commun.* **1989**, 902–903.
(4) Hirschle, C.; Röhr, C. *Z. Anorg. Allg. Chem.* **2000**, *626*, 1305–1312.
(5) Hirschle, C.; Röhr, C. *Acta Crystallogr.* **1998**, *C54*, 1219–1220.
(6) Hoppe, R.; Schwedes, B. *Rev. Chim. Miner.* **1971**, *8*, 583–590.
(7) Keller, E.; Röhr, C. *Z. Kristallogr.* **2008**, *223*, 431–440.
(8) Lee, C.; Harrison, W. T. A. *Acta Crystallogr.* **2004**, *C 60*, m215–m218.
(9) Menary, J. W. *Acta Crystallogr.* **1958**, *11*, 742–743.
(10) Schwedes, B.; Hoppe, R. *Z. Anorg. Allg. Chem.* **1972**, *391*, 313–322.
(11) Schwedes, B.; Hoppe, R. *Z. Anorg. Allg. Chem.* **1972**, *392*, 97–106.
(12) Zoche, N.; Jansen, M. *Z. Anorg. Allg. Chem.* **1998**, *624*, 205–208.
(13) Zoche, N.; Jansen, M. *Z. Anorg. Allg. Chem.* **1997**, *623*, 832–836.
(14) Andersen, N. H.; Poulson, F. W.; Eichinger, G. Studies in Inorganic Chemistry. *Proceedings of the Second European Conference on Solid State Chemistry*, Veldhoven, The Netherlands, June 7−9, 1982; Metselaar, R., Heijligers, H. J. M., Schoonman, J., Eds.; Elsevier: Amsterdam, The Netherlands, 1983; Vol. 3.
(15) Hulliger, F. Physics and Chemistry of Materials with Layered Structures. *Structural Chemistry of Layer-type Phases*; Lévy, F., Ed.; D. Reidel: Dordrecht, Holland, 1976; Vol. 5.
(16) Von Stöver, H.-D.; Hoppe, R. *Z. Anorg. Allg. Chem.* **1980**, *468*, 137–147.
(17) Sauvage, J. P.; Maraine, P.; Perez, G. *C. R. Hebd. Acad. Sci. C* **1976**, *282*, 835–838.
(18) Boultif, A.; Louer, D. *J. Appl. Crystallogr.* **2004**, *37*, 724–731.
(19) Larson, A. C.; Von Dreele, R. B. Los Alamos National Laboratory LAUR 86-748; University of California: Berkeley, CA, 1994.
(20) Toby, B. H. *J. Appl. Crystallogr.* **2001**, *34*, 210–213.
(21) Brown, I. D.; Altermatt, D. *Acta Crystallogr.* **1985**, *B41*, 244–247.